J. Fluid Mech. (1978), *vol.* 84, *part* 3, *pp.* 411–431
Printed in Great Britain

Two-fluid spin-up in a centrifuge

By A. S. BERMAN, J. BRADFORD AND T. S. LUNDGREN
Department of Aerospace Engineering and Mechanics,
University of Minnesota, Minneapolis

(Received 11 March 1976 and in revised form 17 January 1977)

The behaviour of the interface between two immiscible fluids of different density and viscosity in a centrifuge is investigated both analytically and experimentally. The study includes the interfacial shape and behaviour during both steady and transient operation of the centrifuge. The interface shape is investigated for rigid-body rotation and during slow steady acceleration or deceleration of the centrifuge. The dependence of the interface shape on time is investigated during a rapid spin-up to a slightly different value of the angular velocity, which then remains constant. Some aspects of interface stability are also reported.

1. Introduction

The technique of zonal centrifugation, as applied to a variety of problems of biological interest, has developed rapidly during the past decade. Separation of cell components, purification of virus material and isolation of trace amounts of virus present in cells are but a few of the applications recently developed. An early summary of these developments is provided by Anderson (1966). In these applications many modes of centrifuge operation are employed including spin-up of fluids with discrete or continuous density stratification. During spin-up and ultimately during deceleration, various means are employed to prevent bulk mixing effects. These include radial baffles and controlled acceleration and deceleration rates. The fluid mechanics of such devices offers a multitude of problems of interest. An idealized version of one such problem, involving discrete density stratification, is treated in this paper. As has been pointed out by Holton (1965), such a system is also of interest in modelling baroclinic processes involved in atmospheric and oceanic circulations.

In the configuration to be studied a lighter liquid (liquid 1) lies above a heavier liquid (liquid 2) in a cylindrical centrifuge with a flat top and bottom. In one series of experiments the centrifuge rotates with an angular velocity $\Omega(t)$ which is slowly varying with time. If Ω were constant, the interface between the two immiscible liquids would assume a parabolic shape. When Ω depends on time, quite different interfacial shapes can be observed. This is illustrated in figure 14 (plate 1), in which 20 cS oil floats on water in a transparent centrifuge. In figure 14(*e*) the angular velocity is steady and the shape is the equilibrium parabola modified by surface-tension effects. In figure 14(*a*) the angular velocity has about the same value but is slowly increasing with time. The interface has a markedly different, inverted, shape. This is easily understood qualitatively by considering the limiting case where the upper liquid has infinite viscosity and the lower liquid zero viscosity. Then the upper liquid has solid-body velocity at the instantaneous angular velocity while the zero-viscosity liquid slips and remains

at rest. Because of centrifugal forces the pressure in the upper liquid is lower in the centre and higher near the periphery. Therefore the lower liquid tends to rise in the middle, an effect which is more pronounced when the density difference is small. The detailed analysis of this phenomenon is less trivial than this, however.

The equations describing the motion are generalizations of those derived by Pedlosky (1967). The formulation differs in several respects. Pedlosky restricts his analysis to small rotational Froude numbers. In the present treatment substantial variations in Froude number are permitted. In addition fluids of different viscosities are allowed and both rapid spin-up and slow spin-up are included.

In § 2, the equations governing the spatial and temporal development of the interface are obtained. Sections 2.1 and 2.2 treat the transient response of the interface shape to a sudden change in angular acceleration and velocity respectively. The equations describing the interface behaviour during small steady acceleration and deceleration of the centrifuge are obtained in § 2.3. The remaining parts of the paper describe the experimental equipment and the results of experiments.

2. Analysis

If the Ekman number ($E = \nu/\Omega H^2$, H = height of centrifuge) in each liquid is sufficiently small and $\dot{\Omega}$ is sufficiently small, viscous effects are confined to thin Ekman layers at the top and bottom of the centrifuge bowl and on both sides of the curved interface and to thin Stewartson layers along the cylindrical wall.

Equations describing the inviscid interior parts of the liquids may be obtained by linearizing the Euler equations, in cylindrical co-ordinates, about slowly varying solid-body rotation. Denoting the velocity components by $(v_r, r\Omega(t)+v_\theta, v_z)$, where (v_r, v_θ, v_z) are small perturbations from rigid-body rotation, one finds, in each liquid,

$$\rho r\Omega^2 + 2\rho\Omega v_\theta = \partial p/\partial r, \tag{1}$$

$$\partial v_\theta/\partial t + r\dot{\Omega} + 2\Omega v_r = 0, \tag{2}$$

$$\rho g + \partial p/\partial z = 0, \tag{3}$$

$$\partial v_r/\partial r + v_r/r + \partial v_z/\partial z = 0. \tag{4}$$

The terms $\partial v_r/\partial t$ and $\partial v_z/\partial t$ have also been neglected compared with $\partial v_\theta/\partial t$. Equations (1) and (3) imply that v_θ is independent of z, and also determine the pressure once the velocity has been found. Equation (2) gives the radial velocity,

$$v_r = -(2\Omega)^{-1}(r\dot{\Omega} + \partial v_\theta/\partial t), \tag{5}$$

which is independent of z. This does not vanish at the cylindrical walls but feeds fluid into Stewartson layers along this wall. Equation (4), the continuity equation, then shows that v_z is at most a linear function of z. If the position of the interface is denoted by $z = f(r, t)$ this gives

$$v_{z1}(z = f_+) - v_{z1}(z = H) = \left(\frac{\dot{\Omega}}{\Omega} + \frac{1}{2\Omega r}\frac{\partial}{\partial r} r \frac{\partial v_{\theta 1}}{\partial t}\right)(f - H), \tag{6}$$

$$v_{z2}(z = f_-) - v_{z2}(z = 0) = \left(\frac{\dot{\Omega}}{\Omega} + \frac{1}{2\Omega r}\frac{\partial}{\partial r} r \frac{\partial v_{\theta 2}}{\partial t}\right) f, \tag{7}$$

where subscripts 1 and 2 are now used in the upper and lower liquid respectively; $z = 0$ is the bottom and $z = H$ the top of the bowl.

The velocities at the top and bottom are given by the Ekman-suction boundary conditions

$$v_{z1}(z = H) = -\frac{1}{2}\left(\frac{\nu_1}{\Omega}\right)^{\frac{1}{2}} \frac{1}{r}\frac{\partial}{\partial r} r v_{\theta 1}(r, t), \tag{8}$$

$$v_{z2}(z = 0) = \frac{1}{2}\left(\frac{\nu_2}{\Omega}\right)^{\frac{1}{2}} \frac{1}{r}\frac{\partial}{\partial r} r v_{\theta 2}(r, t). \tag{9}$$

The Ekman-suction formulae at the slowly moving interface are more difficult and are derived by solving the viscous Ekman layers on both sides of the interface subject to continuity of velocity and shear stress at the interface. These conditions, which may be deduced from equations given by Greenspan (1969, chap. 2), are

$$v_{z1}(z = f_+) = -\tfrac{1}{2} r \frac{\dot{\Omega}}{\Omega} f' + \frac{\partial f}{\partial t} + \frac{1}{r}\frac{\partial}{\partial r}\frac{r}{2}\left(\frac{\nu_1}{\Omega}\right)^{\frac{1}{2}} (1 + f'^2)^{\frac{1}{4}} \frac{\rho_2 \nu_2^{\frac{1}{2}}}{\rho_1 \nu_1^{\frac{1}{2}} + \rho_2 \nu_2^{\frac{1}{2}}} (v_{\theta 1} - v_{\theta 2}), \tag{10}$$

$$v_{z2}(z = f_-) = -\tfrac{1}{2} r \frac{\dot{\Omega}}{\Omega} f' + \frac{\partial f}{\partial t} + \frac{1}{r}\frac{\partial}{\partial r}\frac{r}{2}\left(\frac{\nu_2}{\Omega}\right)^{\frac{1}{2}} (1 + f'^2)^{\frac{1}{4}} \frac{\rho_1 \nu_1^{\frac{1}{2}}}{\rho_1 \nu_1^{\frac{1}{2}} + \rho_2 \nu_2^{\frac{1}{2}}} (v_{\theta 1} - v_{\theta 2}), \tag{11}$$

where $f' = \partial f/\partial r$. The time derivative of f occurs because one must compute the Ekman suction relative to the moving interface.

When (8)–(11) are substituted into (6) and (7) one obtains

$$\begin{aligned} r\frac{\partial f}{\partial t} - \frac{1}{2}\frac{\dot{\Omega}}{\Omega}\frac{\partial}{\partial r} r^2 (f - H) - \frac{1}{2\Omega}\left[\frac{\partial}{\partial r} r \frac{\partial v_{\theta 1}(r, t)}{\partial t}\right](f - H) \\ = -\frac{\partial}{\partial r}\frac{r}{2}\left(\frac{\nu_1}{\Omega}\right)^{\frac{1}{2}} \left[1 + (1 + f'^2)^{\frac{1}{4}} \frac{\rho_2 \nu_2^{\frac{1}{2}}}{\rho_1 \nu_1^{\frac{1}{2}} + \rho_2 \nu_2^{\frac{1}{2}}}\right] v_{\theta 1}(r, t) \\ + \frac{\partial}{\partial r}\frac{r}{2}\left(\frac{\nu_1}{\Omega}\right)^{\frac{1}{2}} (1 + f'^2)^{\frac{1}{4}} \frac{\rho_2 \nu_2^{\frac{1}{2}}}{\rho_1 \nu_1^{\frac{1}{2}} + \rho_2 \nu_2^{\frac{1}{2}}} v_{\theta 2}(r, t) \end{aligned} \tag{12}$$

and

$$\begin{aligned} r\frac{\partial f}{\partial t} - \frac{1}{2}\frac{\dot{\Omega}}{\Omega}\frac{\partial}{\partial r} r^2 f - \frac{1}{2\Omega}\left[\frac{\partial}{\partial r} r \frac{\partial v_{\theta 2}(r, t)}{\partial t}\right] f \\ = -\frac{\partial}{\partial r}\frac{r}{2}\left(\frac{\nu_2}{\Omega}\right)^{\frac{1}{2}} (1 + f'^2)^{\frac{1}{4}} \frac{\rho_1 \nu_1^{\frac{1}{2}}}{\rho_1 \nu_1^{\frac{1}{2}} + \rho_2 \nu_2^{\frac{1}{2}}} v_{\theta 1}(r, t) \\ + \frac{\partial}{\partial r}\frac{r}{2}\left(\frac{\nu_2}{\Omega}\right)^{\frac{1}{2}} \left[1 + (1 + f'^2)^{\frac{1}{4}} \frac{\rho_1 \nu_1^{\frac{1}{2}}}{\rho_1 \nu_1^{\frac{1}{2}} + \rho_2 \nu_2^{\frac{1}{2}}}\right] v_{\theta 2}(r, t). \end{aligned} \tag{13}$$

These equations relate $v_{\theta 1}$ and $v_{\theta 2}$ to the interface shape function $f(r, t)$, which is not yet known. An additional condition to be imposed is the balance between pressure differences across the interface and surface-tension forces:

$$p_2 - p_1 = -\alpha\left[\frac{f''}{(1 + f'^2)^{\frac{3}{2}}} + \frac{f'}{r(1 + f'^2)^{\frac{1}{2}}}\right], \tag{14}$$

where α is the surface tension. Equations (1) and (3) may be solved for the tangential derivative of the pressure on each side of the interface, whence (14) may be expressed as

$$-\alpha\frac{\partial}{\partial r}\left[\frac{f''}{(1 + f'^2)^{\frac{3}{2}}} + \frac{f'}{r(1 + f'^2)^{\frac{1}{2}}}\right] = -g\Delta\rho\frac{\partial}{\partial r}\left(f - \frac{1}{2}\frac{r^2\Omega^2}{g}\right) + 2\rho_2\,\Omega v_{\theta 2} - 2\rho_1\,\Omega v_{\theta 1}, \tag{15}$$

where $\Delta\rho = \rho_2 - \rho_1 > 0$.

Equations (12), (13) and (15) constitute three equations for the three unknown functions $v_{\theta 1}$, $v_{\theta 2}$ and f. These are to be solved subject to the condition that the contact angle η of the interface with the wall be specified:

$$\tan\eta = \partial f/\partial r \quad \text{at} \quad r = a, \tag{16}$$

where η is the angle between the normal to the interface and the axis of the centrifuge. A second condition is that the volume occupied by each liquid remains constant. This is

$$2\pi \int_0^a rf\,dr = \pi a^2 H_0, \tag{17}$$

where a is the radius of the centrifuge and H_0 is the mean height of the interface.

2.1. *Decay of transients*

In an attempt to understand better the time scales involved, a transient problem will be considered. If the acceleration rate which produced figure 14(*a*) is suddenly reduced to zero, how long will it take for the interface to decay to that shown in figure 14(*e*)? Qualitatively, the dropping interface squeezes liquid into the Ekman layers, where it flows radially to conserve mass and meets viscous resistance to flow.

To simplify the problem as much as possible, surface tension will be neglected and it will be assumed that $\nu_1 \to \infty$, so that $v_{\theta 1} = 0$. (In the experiments $\nu_1 \geqslant 20\nu_2$.) Then, with $\dot{\Omega} = 0$, (13) and (15) become

$$r\frac{\partial f}{\partial t} - \frac{1}{2\Omega}\left(\frac{\partial}{\partial r} r \frac{\partial v_{\theta 2}}{\partial t}\right) f = \frac{\partial}{\partial r}\frac{r}{2}\left(\frac{\nu_2}{\Omega}\right)^{\frac{1}{2}} [1 + (1+f'^2)^{\frac{1}{2}}]\, v_{\theta 2}, \tag{18}$$

$$0 = -g\Delta\rho \frac{\partial}{\partial r}\left(f - \frac{1}{2}\frac{r^2\Omega^2}{g}\right) + 2\rho_2 \Omega v_{\theta 2}. \tag{19}$$

Using (19) to eliminate $v_{\theta 2}$ from (18) gives

$$r\frac{\partial f}{\partial t} - \frac{f}{2\Omega}\frac{g\Delta\rho}{2\rho_2\Omega}\frac{\partial}{\partial t}\frac{\partial}{\partial r} r \frac{\partial}{\partial r}\left(f - \frac{1}{2}\frac{r^2\Omega^2}{g}\right)$$

$$= \frac{1}{2}\left(\frac{\nu_2}{\Omega}\right)^{\frac{1}{2}} \frac{g\Delta\rho}{2\rho_2\Omega}\frac{\partial}{\partial r} r[1 + (1+f'^2)^{\frac{1}{2}}]\frac{\partial}{\partial r}\left(f - \frac{r^2\Omega^2}{2g}\right), \tag{20}$$

a single nonlinear partial differential equation for f.

In the steady state the only bounded solution is

$$f - r^2\Omega^2/2g = \text{constant},$$

which is the equilibrium parabola with the constant of integration to be determined from (17). It is convenient to use a new independent variable $\zeta = r/a$ and a new dependent variable

$$F = (f/a) - (H_0/a) + \tfrac{1}{2}N_F(\tfrac{1}{2} - \zeta^2), \tag{21}$$

where

$$N_F = a^2\Omega^2/ag \tag{22}$$

is a rotational Froude number. This new variable has the property

$$\int_0^1 \zeta F\,d\zeta \equiv 0 \tag{23}$$

in the steady state and more generally measures the deviation from the equilibrium parabola.

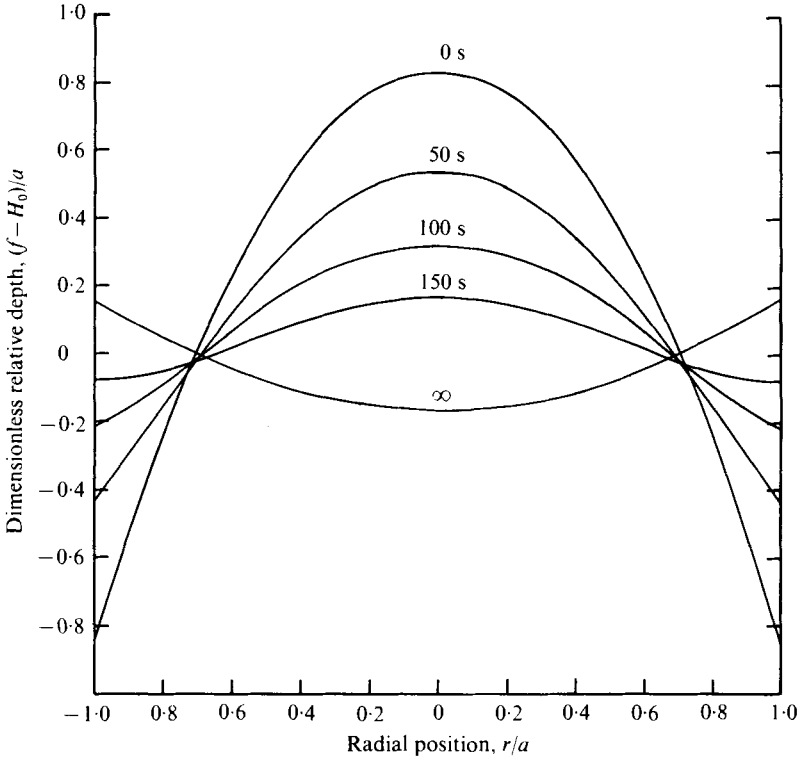

FIGURE 1. Decay of interface shape from a state of steady acceleration for water and 20 cS silicone oil [equation (29)]. Curves correspond to times $t = 0$, 50 s, 100 s, 150 s and ∞. Compare with figure 14.

It is also convenient to introduce an internal rotational Froude number

$$N_I = N_F \rho_2/(\rho_2 - \rho_1), \tag{24}$$

a dimensionless time

$$t_2 = \Omega(\nu_2/a^2\Omega)^{\frac{1}{2}} t(2N_I)^{-1} \tag{25}$$

and a dimensionless parameter

$$\lambda = (H_0/a)\,(4N_I)^{-1}. \tag{26}$$

Equation (20) can now be written

$$\zeta\frac{\partial F}{\partial t_2} - \frac{\lambda f}{H_0}\frac{\partial}{\partial\zeta}\zeta\frac{\partial}{\partial\zeta}\frac{\partial F}{\partial t_2} = \frac{\partial}{\partial\zeta}\zeta\frac{1+(1+f'^2)^{\frac{1}{2}}}{2}\frac{\partial F}{\partial\zeta}. \tag{27}$$

In order to proceed, two approximations will be made:

$$f/H_0 \cong 1, \quad \tfrac{1}{2}[1+(1+f'^2)^{\frac{1}{2}}] \cong 1. \tag{28}$$

These would be exact for a flat interface and should not introduce too much error for the cases to be studied experimentally because of the large depth-to-radius ratio of the bowl and the reducing effect of the quarter power.

With these approximations (27) becomes linear and may be solved by separation of variables to give

$$F = \sum_{n=1}^{\infty} A_n \exp\left(-\frac{j_{1,n}\, t_2}{1+\lambda j_{1,n}^2}\right) J_0(j_{1,n}\zeta), \tag{29}$$

where J_0 is a zeroth-order Bessel function and $j_{1,n}$ is the nth root of J_1, i.e. $J_1(j_{1,n}) = 0$. The Bessel function has the property

$$\int_0^1 \zeta J_0(j_{1,n}\zeta)\,d\zeta = 0$$

therefore (23) is satisfied. The coefficients A_n can be determined from the initial values by using the orthogonality of the Bessel functions.

The e-folding time, computed from the largest exponent in (29), is from one to several minutes depending on the angular velocity.

The decaying interface shape calculated from (29) for a special case is shown in figure 1 and should be compared with the sequence of figures 14 (*a*)–(*e*). The coefficients A_n were determined by analysis of the initial shape, from a photograph, at the start of the decay. The details of the experiment will be discussed in a later section.

From (19) one finds that the velocity

$$\frac{v_{\theta 2}}{a\Omega} = \frac{1}{2N_I}\frac{\partial F}{\partial \zeta}. \tag{30}$$

The basic linearization which produced (1)–(4) required that this quantitity be small ($v_\theta \ll r\Omega$). This requires that the internal Froude number N_I be large, a condition that was easily satisfied in the experiments. Since $\partial F/\partial\zeta$ is negative in these experiments, the flow rotates more slowly than the bowl. This sense of rotation is required in order for the fluid between the dropping interface and the bottom to be squeezed into the Ekman layers.

2.2. *Step spin-up*

The response of the fluid to an instantaneous spin-up of the centrifuge from an initial angular velocity $\Omega - \Delta\Omega$ to a final angular velocity Ω is also described by (12), (13) and (15) provided $\Delta\Omega/\Omega$ is small. In this case one sets $\dot{\Omega} = 0$ and lets $v_{\theta 1}$, $v_{\theta 2}$ and F be the perturbations from the final spun-up state. The initial conditions are then calculated from the initial state:

$$\left.\begin{aligned} v_{\theta 1}/a\Omega = v_{\theta 2}/a\Omega &= -\zeta(\Delta\Omega/\Omega), \\ F &= (\tfrac{1}{2} - \zeta^2)\,N_F(\Delta\Omega/\Omega). \end{aligned}\right\} \tag{31}$$

The case where the viscosity of the upper fluid is much larger than that of the lower fluid is of particular interest. This problem has two characteristic times. There is a short time period during which the upper fluid rapidly spins up to its final state and the interface shape adjusts to this new situation. The rapidly changing interface also induces a motion in the lower fluid. This initial phase is followed by a slower decay of the lower fluid to the final state. This phase is described by the transient decay problem of § 2.1.

Analytically the problem is a singular perturbation problem requiring an initial 'boundary layer'. If one scales the time by the dimensionless time t_2 defined by (25), the small parameter $(\nu_2/\nu_1)^{\frac{1}{2}}$ will appear before the time-derivative terms on the left-hand side of (12). If one then takes the limit as this parameter tends to zero (12) yields $v_{\theta 1} = 0$ and then (13) and (15) give (27). It is clear that $v_{\theta 1} = 0$ does not satisfy the initial conditions of the problem for the classical reason of a small parameter premultiplying one of the highest derivative terms. One may eliminate this problem by rescaling so as

to absorb the small parameter into a new time variable. To this end introduce the dimensionless time

$$t_1 = \Omega t[\nu_1/\Omega(H-H_0)^2]^{\frac{1}{2}}, \tag{32}$$

which scales the time with the spin-up time for fluid 1 alone. Introduce

$$v_1 = v_{\theta 1}/a\Omega, \quad v_2 = v_{\theta 2}/a\Omega \tag{33}$$

and F, defined by (21). If surface tension is neglected and the approximations indicated by (28) are made, (12), (13) and (15) may be written (with $\psi = (\nu_2/\nu_1)^{\frac{1}{2}}$) as

$$\frac{a}{H-H_0}\zeta\frac{\partial F}{\partial t_1}+\frac{1}{2}\frac{\partial}{\partial\zeta}\zeta\frac{\partial v_1}{\partial t_1} = -\frac{1}{2}\frac{\partial}{\partial\zeta}\zeta\left(1+\frac{(\rho_2/\rho_1)\psi}{1+(\rho_2/\rho_1)\psi}\right)v_1+\frac{1}{2}\frac{\partial}{\partial\zeta}\zeta\frac{(\rho_2/\rho_1)\psi}{1+(\rho_2/\rho_1)\psi}v_2, \tag{34}$$

$$\frac{a}{H-H_0}\zeta\frac{\partial F}{\partial t_1}-\frac{H_0}{H-H_0}\frac{1}{2}\frac{\partial}{\partial\zeta}\zeta\frac{\partial v_2}{\partial t_1} = \frac{-\psi}{1+(\rho_2/\rho_1)\psi}\frac{1}{2}\frac{\partial}{\partial\zeta}\zeta v_1+\psi\left(\frac{1}{1+(\rho_2/\rho_1)\psi}\right)\frac{1}{2}\frac{\partial}{\partial\zeta}\zeta v_2, \tag{35}$$

$$v_2 = (\rho_1/\rho_2)v_1+(1/2N_I)(\partial F/\partial\zeta). \tag{36}$$

In the limit $\psi = (\nu_2/\nu_1)^{\frac{1}{2}}\to 0$, the right-hand side of (35) is zero and it may be integrated once with respect to time, giving

$$\zeta F-\frac{1}{2}\frac{H_0}{a}\frac{\partial}{\partial\zeta}\zeta v_2 = \zeta(\tfrac{1}{2}-\zeta)^2N_F\frac{\Delta\Omega}{\Omega}+\frac{H_0}{a}\zeta\frac{\Delta\Omega}{\Omega}, \tag{37}$$

where the initial conditions (31) have been used.

The limiting form of (34) is

$$\frac{a}{H-H_0}\zeta\frac{\partial F}{\partial t_1}+\frac{1}{2}\frac{\partial}{\partial\zeta}\zeta\frac{\partial v_1}{\partial t_1}+\frac{1}{2}\frac{\partial}{\partial\zeta}\zeta v_1 = 0 \tag{38}$$

and when (36) is used to eliminate v_2 from (37) the following equation results:

$$\zeta F-\frac{1}{2}\frac{H_0}{a}\frac{\rho_1}{\rho_2}\frac{\partial}{\partial\zeta}\zeta v_1-\lambda\frac{\partial}{\partial\zeta}\zeta\frac{\partial F}{\partial\zeta} = \zeta(\tfrac{1}{2}-\zeta^2)N_F\frac{\Delta\Omega}{\Omega}+\frac{H_0}{a}\zeta\frac{\Delta\Omega}{\Omega}. \tag{39}$$

This pair of equations, with initial conditions given by (31) and the conservation-of-volume condition (23), may readily be solved for v_1 and F. A solution for F is sought which is the sum of a steady part and a transient part. Separation of variables then leads to

$$F = F_s+\sum_{n=1}^{\infty}B_nJ_0(j_{1,n}\zeta)\exp(-\phi_nt_1), \tag{40}$$

$$v_1 = \frac{2}{H_0/a}\frac{\rho_2}{\rho_1}\sum_{n=1}^{\infty}\frac{1+\lambda j_{1,n}^2}{j_{1,n}}B_nJ_1(j_{1,n}\zeta)\exp(-\phi_nt), \tag{41}$$

where

$$\phi_n = (1+\lambda j_{1,n}^2)\Big/\left[1+\frac{\rho_1}{\rho_2}\frac{H_0}{H-H_0}+\lambda j_{1,n}^2\right], \tag{42}$$

$$F_s = \left[(\tfrac{1}{2}-\zeta^2)N_F+\frac{\rho_1}{\rho_2}\frac{H_0}{a}\right]\frac{\Delta\Omega}{\Omega}-\frac{1}{2}\frac{\rho_1}{\rho_2}\frac{H_0}{a}\frac{\Delta\Omega}{\Omega}\frac{I_0(\lambda^{-\frac{1}{2}}\zeta)}{\lambda^{\frac{1}{2}}I_1(\lambda^{-\frac{1}{2}})}, \tag{43}$$

I_0 and I_1 are modified Bessel functions and the coefficients B_n are determined from the initial conditions. When $\rho_2-\rho_1$ is small the numbers ϕ_n satisfy $(H-H_0)/H < \phi_n < 1$

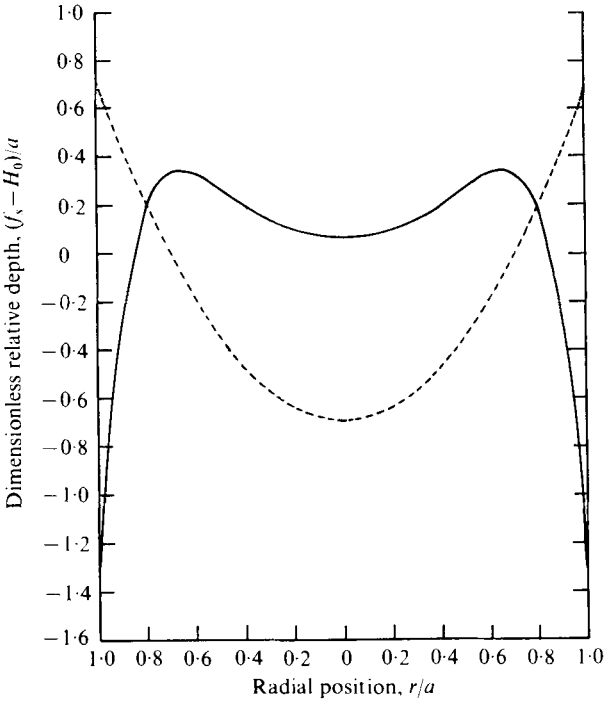

FIGURE 2. Short-time asymptotic interface shape for step spin-up of water and 350 cS silicone oil [from (44)]; $\Omega = 204$ r.p.m., $\dot{\Omega} = 0{\cdot}1$, $H_0/H = 0{\cdot}5$. Dotted line corresponds to rigid-body rotation at 204 r.p.m. Compare with figure 15.

and when λ is small they tend to be close to the lower bound for the lower modes and near the upper bound for sufficiently large n. Therefore it is clear that in a time comparable to the spin-up time of the upper fluid $v_1 \to 0$, $F \to F_s$ and, from (36), $v_2 \to (2N_I)^{-1} \partial F_s / \partial \zeta$. By the concepts of matched asymptotic expansions this short-time asymptote provides the initial conditions for the further slow decay to the ultimate spin-up state. That is, F_s provides the initial conditions for the calculation of the coefficients A_n in (29).

The short-time asymptotic interface shape is given by

$$f_s/a - H_0/a = F_s + \tfrac{1}{2}(\zeta^2 - \tfrac{1}{2})\, N_F \tag{44}$$

and is not simply a small perturbation from the equilibrium shape when λ is small. From (43) it can be seen that, in this case, the interface bulges up in the middle with a corresponding deep boundary layer near the bowl wall with thickness of order $\lambda^{\frac{1}{2}}$. This is shown in figure 2 for 350 cS oil (with $(\rho_2 - \rho_1)/\rho_2 = 0{\cdot}028$) over water with $\Omega = 204$ r.p.m. and $H_0/a = 0{\cdot}5$, which makes $\lambda = 0{\cdot}015$. This is to be compared with figure 15 (plate 2), which shows a photograph taken 20 s after initiation of spin-up under the same conditions.

From (44) one can calculate the rise of the centre-line height above its initial position for rigid-body rotation at angular velocity $\Omega - \Delta\Omega$. This is found to be

$$\frac{\rho_1}{\rho_2}\frac{H_0}{H}\frac{\Delta\Omega}{\Omega}\left(1 - \frac{1}{2}\frac{\lambda^{-\frac{1}{2}}}{I_1(\lambda^{-\frac{1}{2}})}\right), \tag{45}$$

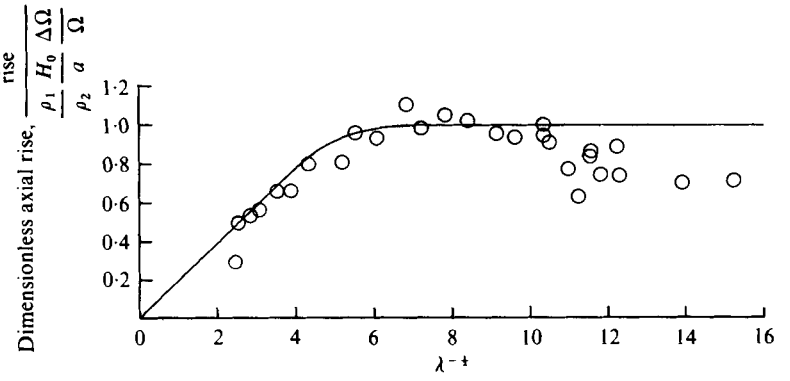

FIGURE 3. Maximum axial rise of interface during step spin-up for water and 350 cS silicone oil; $H_0/H = 0{\cdot}5$.

which is approximately

$$\frac{\rho_1}{\rho_2}\frac{H_0}{H}\frac{\Delta\Omega}{\Omega}$$

when λ is small. This compares with the ultimate *drop* of the centre-line height by the amount $\frac{1}{2}N_F\,\Delta\Omega/\Omega$. Measurements of centre-line rise have been performed for a range of Ω for the 350 cS oil and are compared with (45) in figure 3.

2.3. *Quasi-steady solution*

A major goal of this paper is to study the interfacial shape during a slow spin-up. If the characteristic relaxation time of the last section is small compared with the characteristic time for changes in Ω, namely $\Omega/\dot{\Omega}$, then the problem may be simplified by neglecting the terms $\partial f/\partial t$, $\partial v_{\theta 1}/\partial t$ and $\partial v_{\theta 2}/\partial t$ in (12) and (13). Furthermore the surface tension may be neglected as a first approximation and the approximations of (28) may be made. This will be done in an orderly fashion by making use of a multiple perturbation expansion.

Attention will be restricted to the situation where $\dot{\Omega}$ is constant. After an initial transient has decayed away, the solution will depend on time only through its dependence on Ω and a dimensionless time $T = \ln \Omega$ may be introduced with the properties

$$\frac{\partial}{\partial t} = \frac{\dot{\Omega}}{\Omega}\frac{\partial}{\partial T}, \quad \frac{\partial}{\partial T} = \Omega\frac{\partial}{\partial \Omega}. \tag{46}$$

The dimensionless variable F defined by (21) is used and dimensionless velocities are defined by

$$V_1 = N_I v_{\theta 1}/a\Omega = N_I v_1, \tag{47}$$

$$V_2 = N_I v_{\theta 2}/a\Omega = N_I v_2. \tag{48}$$

For the purpose of this section, a further simplification is made by assuming $\rho_1 = \rho_2 = \rho$ everywhere except in (15), where the difference $\Delta\rho$ is multiplied by the gravitational acceleration g.

An additional small parameter β, which is essentially the ratio of the relaxation time given in (25) to the characteristic time $\Omega/\dot{\Omega}$, is defined by

$$\beta = \frac{1}{2}\frac{\dot{\Omega}}{\Omega^2} N_I \left[\left(\frac{a^2\Omega}{\nu_1}\right)^{\frac{1}{2}} + \left(\frac{a^2\Omega}{\nu_2}\right)^{\frac{1}{2}}\right] \tag{49}$$

and a small surface-tension parameter is introduced by the definition

$$\delta^2 = \alpha/ga^2\Delta\rho.$$

The notation

$$S = 1 + (df/dr)^2 = 1 + (\partial F/\partial\zeta + N_F\zeta)^2, \tag{50}$$

$$\Gamma = S^{\frac{1}{2}} - 1 \tag{51}$$

is adopted for convenience.

With these new variables (12), (13) and (15) may be written as

$$-\frac{\partial}{\partial\zeta}\zeta\left(\frac{\nu_1^{\frac{1}{2}}+\nu_2^{\frac{1}{2}}}{\nu_2^{\frac{1}{2}}} + 1 + \epsilon\Gamma\right) V_1 + \frac{\partial}{\partial\zeta}\zeta(1+\epsilon\Gamma)\, V_2$$

$$= 4\beta\left(-\tfrac{1}{4}N_F + \frac{H}{a} - \frac{H_0}{a}\right)\zeta + 4\beta\left(\zeta\frac{\partial F}{\partial T} - \frac{1}{2}\frac{\partial}{\partial\zeta}\zeta^2 F\right)$$

$$-\frac{2\beta}{N_I}\left[\frac{\partial}{\partial\zeta}\zeta\left(\frac{\partial V_1}{\partial T} - V_1\right)\right]\left(F - \frac{H}{a} + \frac{H_0}{a} + \tfrac{1}{2}N_F\zeta^2 - \tfrac{1}{4}N_F\right), \tag{52}$$

$$-\frac{\partial}{\partial\zeta}\zeta(1+\epsilon\Gamma)\, V_1 + \frac{\partial}{\partial\zeta}\zeta\left(\frac{\nu_1^{\frac{1}{2}}+\nu_2^{\frac{1}{2}}}{\nu_1^{\frac{1}{2}}} + 1 + \epsilon\Gamma\right) V_2$$

$$= -4\beta\left(\tfrac{1}{4}N_F + \frac{H_0}{a}\right)\zeta + 4\beta\left(\zeta\frac{\partial F}{\partial T} - \frac{1}{2}\frac{\partial}{\partial\zeta}\zeta^2 F\right)$$

$$-\frac{2\beta}{N_I}\left[\frac{\partial}{\partial\zeta}\zeta\left(\frac{\partial V_2}{\partial T} - V_2\right)\right]\left(F + \frac{H_0}{a} + \tfrac{1}{2}N_F\zeta^2 - \tfrac{1}{4}N_F\right), \tag{53}$$

$$2(V_2 - V_1) - \frac{\partial F}{\partial\zeta} = -\delta^2\frac{\partial}{\partial\zeta}\left[\frac{(\partial^2 F/\partial\zeta^2 + N_F)}{S^{\frac{3}{2}}} + \frac{(\partial F/\partial\zeta + N_F\zeta)}{\zeta S^{\frac{1}{2}}}\right], \tag{54}$$

which are to be solved with the boundary condition, obtained from (16),

$$\partial F/\partial\zeta = \tan\eta - N_F$$

and subject to the conservation condition (23). The parameter ϵ is unity. It is introduced as an artificial expansion parameter to reflect the fact that Γ itself is small. It will be noted that the scaling has been chosen such that F, V_1 and V_2 are all of the same order of magnitude. Since Γ, β, β/N_I and δ^2 are all small and $\partial/\partial T = \Omega\,\partial/\partial\Omega$ does not introduce an order change, the terms which determine this magnitude are the first terms on the right-hand sides of (52) and (53), which are of order one or less. For our experiments, the ranges of the parameters introduced above are given in §4.2.

A solution is sought in the form of a perturbation expansion in these small parameters which will be terminated after the first-order terms, neglecting squares and products of these parameters. The part of the perturbation expansion associated with the surface-tension parameter δ is singular since δ^2 multiplies the highest derivative in

(54) and this necessitates a boundary layer with thickness of order δ. The expansion may be written as

$$F = F^{(0)} + \epsilon F^{(1)} + \beta F^{(2)} + \frac{\beta}{N_I} F^{(3)} + \delta^2 F^{(4)} + \delta G\left(\frac{1-\zeta}{\delta}\right) + \ldots, \tag{55}$$

with similar expansions for V_1, V_2, S and Γ. The last term in the expansion is a boundary-layer correction which is transcendentally small except near the bowl wall $\zeta = 1$.

It is a straightforward matter to solve (52) and (52) for the zeroth-order velocities:

$$V_1^{(0)} = \beta\zeta \frac{\nu_2^{\frac{1}{2}}}{\nu_1^{\frac{1}{2}} + \nu_2^{\frac{1}{2}}} \left[\tfrac{1}{4}N_F + \frac{H_0}{a} - \frac{H}{a}\left(1 + \frac{\nu_1^{\frac{1}{2}}}{\nu_1^{\frac{1}{2}} + \nu_2^{\frac{1}{2}}}\right)\right] \tag{56}$$

and

$$V_2^{(0)} = -\beta\zeta \frac{\nu_1^{\frac{1}{2}}}{\nu_1^{\frac{1}{2}} + \nu_2^{\frac{1}{2}}} \left[\tfrac{1}{4}N_F + \frac{H_0}{a} + \frac{H}{a}\frac{\nu_2^{\frac{1}{2}}}{\nu_1^{\frac{1}{2}} + \nu_2^{\frac{1}{2}}}\right]. \tag{57}$$

Using these expressions in (54) yields

$$F^{(0)} = -\beta(\zeta^2 - \tfrac{1}{2})\tilde{H} \quad \text{with} \quad \tilde{H} = \tfrac{1}{4}N_F + \frac{H_0}{a} - \frac{\nu_2^{\frac{1}{2}}}{\nu_1^{\frac{1}{2}} + \nu_2^{\frac{1}{2}}}\frac{H}{a}. \tag{58}$$

This parabolic function opens downwards if β is positive (spin-up) and $\tilde{H}$ is positive ($\nu_1^{\frac{1}{2}} \gg \nu_2^{\frac{1}{2}}$). The effect of this when added to the equilibrium profile

$$f/a = \tfrac{1}{2}N_F(\zeta^2 - \tfrac{1}{2}) + H_0/a$$

leads to the observed inverted shapes if $\beta\tilde{H} > \frac{1}{2}N_F$. Since β must be small this may be best achieved for moderate or small Froude number and large H_0/a. From (56) and (57) it is seen that the velocities in both fluids are solid-body rotations at angular velocities slightly different from that of the centrifuge. If β is positive and $\nu_1 \gg \nu_2$ the lower fluid rotates more slowly than the upper fluid.

Similarly the first-order terms $F^{(1)}$, $F^{(2)}$ and $F^{(3)}$ are easily found to be

$$F^{(1)} = \tfrac{1}{2}\beta\tilde{H}\left\{\frac{4}{5\gamma^2}(1+\gamma^2\zeta^2)^{\frac{5}{4}} - \frac{16}{45\gamma^4}[(1+\gamma^2)^{\frac{9}{4}} - 1] + \tfrac{1}{2} - \zeta^2\right\}, \tag{59}$$

where

$$\gamma = N_F - 2\beta\tilde{H}, \tag{60}$$

$$F^{(2)} = \beta(\tfrac{3}{8}\tilde{H} - \tfrac{1}{8}N_F)\zeta^4 + \beta(-\tfrac{1}{4}\tilde{H} + \tfrac{1}{4}N_F)\zeta^2 - \tfrac{1}{12}\beta N_F \tag{61}$$

and

$$\begin{aligned} F^{(3)} = \frac{4\beta}{(\nu_1^{\frac{1}{2}} + \nu_2^{\frac{1}{2}})^2}\Bigg\{\nu_2\Bigg[-\frac{3N_F}{8} + \frac{H_0}{2a} - \frac{H}{2a}\left(1 + \frac{\nu_1^{\frac{1}{2}}}{\nu_1^{\frac{1}{2}} + \nu_2^{\frac{1}{2}}}\right)\Bigg]\Bigg[\frac{1}{4}\left(\frac{\beta\tilde{H}}{2} - \frac{H}{a} + \frac{H_0}{a} - \frac{N_F}{4}\right)(\zeta^2 - \tfrac{1}{2}) \\ + \frac{1}{16}\left(-\beta\tilde{H} + \frac{N_F}{2}\right)(\zeta^4 - \tfrac{1}{3})\Bigg] - \nu_1\Bigg[-\frac{3N_F}{8} + \frac{H_0}{2a} + \frac{H}{2a}\frac{\nu_2^{\frac{1}{2}}}{\nu_1^{\frac{1}{2}} + \nu_2^{\frac{1}{2}}}\Bigg] \\ \times\left[\frac{1}{4}\left(\frac{\beta\tilde{H}}{2} - \frac{N_F}{4} + \frac{H_0}{a}\right)(\zeta^2 - \tfrac{1}{2}) + \frac{1}{16}\left(-\beta\tilde{H} + \frac{N_F}{2}\right)(\zeta^4 - \tfrac{1}{3})\right]\Bigg\}. \end{aligned} \tag{62}$$

The function $F^{(4)}$ is the surface-tension correction in the interior of the fluid and is given by

$$F^{(4)} = \frac{\gamma}{(1+\gamma^2\zeta^2)^{\frac{3}{2}}} + \frac{\gamma}{(1+\gamma^2\zeta^2)^{\frac{1}{2}}} + C_4, \tag{63}$$

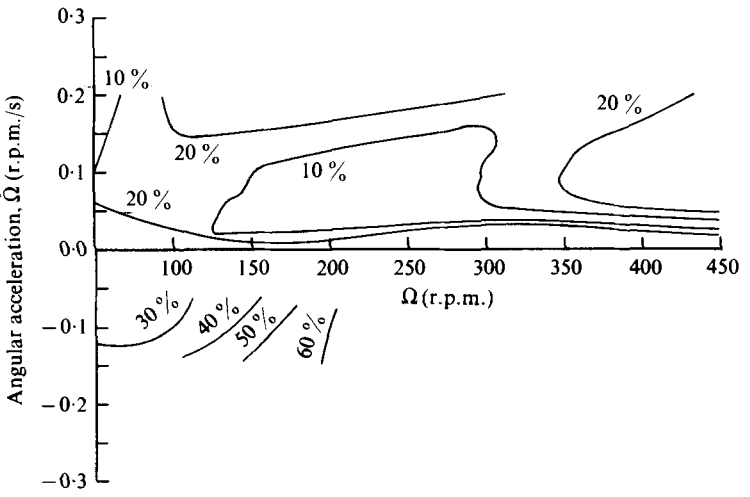

FIGURE 4. Contour lines of percentage contribution of first-order perturbation terms to the zero-order solution $F^{(0)}$ on the axis; water and 20 cS oil, $H_0/H = 0{\cdot}6$. Example: $\Omega = 150$ r.p.m., $\dot{\Omega} = 0{\cdot}1$ r.p.m./s, $[(F^{(1)} + \beta F^{(2)} + (\beta/N_I)\, F^{(3)} + \delta^2 F^{(4)})/F^{(0)}] = 0{\cdot}1$.

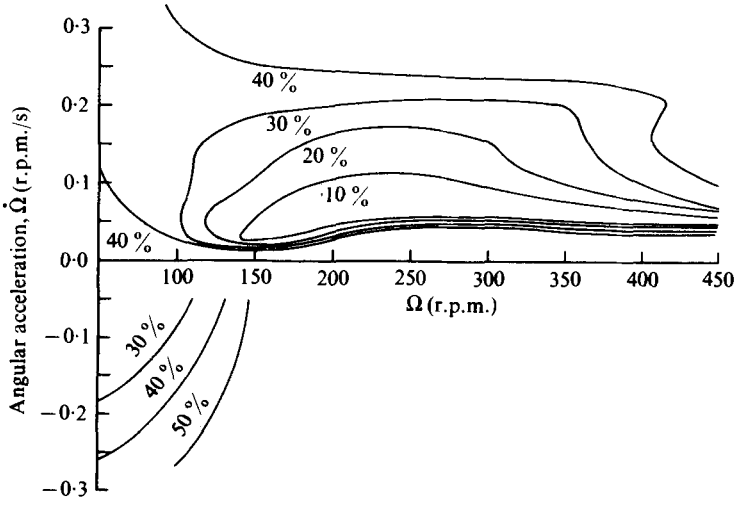

FIGURE 5. Contour lines of percentage contribution of first-order perturbation terms to the zero-order solution $F^{(0)}$ on the axis; water and 350 cS oil; $H_0/H = 0{\cdot}25$.

where the constant of integration C_4 must be so determined that (23) is satisfied, with the boundary layer included.

To treat the boundary layer, introduce the new variables $\xi = (1-\zeta)/\delta$ and $G(\xi)$ defined by (55). Substituting (55) into the boundary condition and into (54) gives, respectively,

$$\left.\frac{dG}{d\xi}\right|_{\xi=0} = \gamma - \tan\eta \tag{64}$$

and

$$\frac{dG}{d\xi} = \frac{d}{d\xi}\frac{d^2G/d\xi^2}{[1+(\gamma - dG/d\xi)^2]^{\frac{3}{2}}}. \tag{65}$$

The latter equation may be integrated once, giving

$$G = \frac{d^2G/d\xi^2}{[1+(\gamma-dG/d\xi)^2]^{\frac{3}{2}}} = \frac{d}{d\xi}\int^{dG/d\xi-\gamma} \frac{d\phi}{(1+\phi^2)^{\frac{3}{2}}}, \tag{66a, b}$$

where the constant of integration must be zero in order for the solution to be bounded at infinity. This equation is too difficult to solve in closed form, but enough information can be obtained to evaluate the constant C_4.

The condition imposed by (23) may be written as

$$0 = \int_0^1 \zeta F^{(4)}\, d\zeta + \int_0^\infty G(\xi)\, d\xi. \tag{67}$$

This integral may be evaluated by using (66*b*) and the boundary condition (64). This gives

$$\int_0^\infty G\, d\xi = \sin\eta - \frac{\gamma}{(1+\gamma^2)^{\frac{1}{2}}}. \tag{68}$$

Equation (67) then yields

$$C_4 = -2\sin\eta,$$

thus completing the expression for $F^{(4)}$.

All of the above corrections are typically of order 5–10 % of F_0 over most of the operating range but they can be as large as 20 % or more under extreme operating conditions. Figures 4 and 5 indicate the contributions made by the perturbation terms to the axial position of the surface. Along any contour indicated in these figures the fractional contribution of the perturbation terms is constant. From the figures one can decide whether a given pair of operating parameters (Ω, $\dot{\Omega}$) is such that the results of the experiment should be reasonably described by the perturbation analysis.

3. Experimental equipment

The centrifuge used in these experiments consists of a right circular cylinder cut from a standard lucite pipe. The section used was carefully selected for concentricity and uniformity of wall thickness and has a length of 73·15 cm between the end plates, an inside radius of 6 cm and a wall thickness of 1·27 cm. The end plates are threaded disks which screw into matching threads machined in the centrifuge bowl wall. Sealing is accomplished with O-rings. The end plates are also fitted with shafts which rotate in oil-lubricated, water-cooled bearings. The lower bearing is provided with appropriate damping to minimize any oscillations resulting from slight imbalance in the bowl. The centrifuge bowl is suspended via the upper shaft from the rotor of the air turbine which provides the motive power for driving the centrifuge. The turbine rotor is fitted with a magnetic pick-up which produces a signal used for monitoring and controlling the speed of rotation. The magnetic pick-up provides six pulses per revolution. These pulses, after shaping and amplification, are counted by a conventional electronic digital counter, for preselected intervals of time, to provide a measure of the rotational speed. The same pulses are also used for speed control by comparing them with an internally generated signal, preset for a desired speed, and using the difference signal to adjust the air supply to the turbine driving the centrifuge. This scheme results in speed control of about $\pm$ 1 r.p.m. at all rotational speeds of operation. Electronic con-

trol circuits allow operation of the centrifuge either at a constant preselected speed or at preselected rates of acceleration or deceleration. Two proximity probes, one near the top of the bowl and the other near the bottom of the bowl, permit monitoring of the excursions of the bowl ends from a state of pure rotation about the geometric axis of the bowl. With the exception of the lucite bowl with modified end plates used in our experiments, all the centrifuge components and electronic controls have been described in detail by Anderson (1966).

The liquids used were distilled water and Dow Silicone oil. Temperatures were measured with a calibrated thermocouple before and after a run and the average temperature used for computation of water and oil viscosities. Surface and interfacial tensions of the liquids were measured with a DeNouy tensiometer. Heights of interface surface points relative to a selected reference level were measured with a cathetometer.

In all of the experiments to be discussed, the upper part of the centrifuge contained either 20 cS or 350 cS silicone oil (specific gravity = 0·955 and 0·972 respectively) while the lower part contained demineralized water.

After completion of the experiments, oil and water from the neighbourhood of the interface were removed from the centrifuge and the surface and interfacial tensions were determined. For water and air, a surface tension of 49·14 dyn/cm was found while for 20 cS oil and air, 20·15 dyn/cm was obtained. The interfacial tension for the 20 cS oil and water was found to be 28·0 dyn/cm. For water and 350 cS oil the interfacial tension was found to be 31·18 dyn/cm. Wetting angles were estimated by observation of the interface in the centrifuge. The rather low surface tension for the water is attributed to traces of surface-active agents remaining on the inner lucite wall of the centrifuge, which had been cleaned, rinsed with demineralized water and dried after machining.

4. Experimental results and discussion

4.1. *Rigid-body rotation*

To investigate the effects of interfacial tension on the interface between the water and oil, measurements were made of the steady-state axial depth of the interface at various constant rotational speeds from 50 to 400 r.p.m. At each speed, the two fluids were permitted to attain rigid-body rotation and an average value of the axial depth of the interface relative to its position at rest ($f = H_0$) was determined. The axial depth of the interface is very sensitive to small accelerations or decelerations. These result from slight variations in rotational speed introduced by pressure variations in the primary air supply and associated drift in the present signal used to control rotational speed. Because of this problem, the depth of the axial interface point was measured at intervals during the approach to rigid-body rotation and for about 20–30 min after achievement of rigid-body rotation. The average position obtained from the latter measurements was taken to be the position of the axial interface point for rigid-body rotation.

The results of such measurements for 20 cS oil and water are shown in figure 6, which gives the axial depth of the interface relative to its rest position for various rotational speeds. Also shown in the figure are the predicted depths computed from (55) with $\hat{\Omega}$ set equal to zero. These curves show the prediction obtained if one neglects surface tension and also the result of using an interfacial tension of 28·0 dyn/cm and a wetting

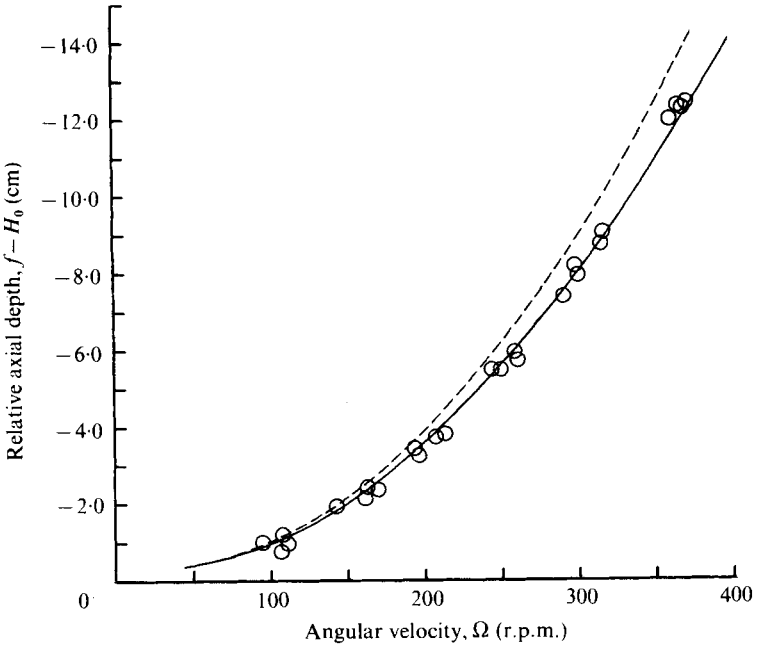

FIGURE 6. Interface axial depth in rigid-body rotation. ——, calculated using $\alpha = 28{\cdot}0$ dyn/cm; ------, calculated using $\alpha = 0$.

angle of 60°. Fortunately, the calculated curve is relatively insensitive to the wetting angle, so that estimates of this angle from direct observation of the interface in the centrifuge were sufficient. As can be seen in the figure, the effect of interfacial tension is clearly outside experimental scatter at the higher rotational speed, where the curvature of the interface is greatest.

As indicated by the definition of δ^2 following (49), the effect of surface tension is inversely proportional to the density difference of the fluids and hence the effect is expected to be observable for our system. By the same argument, surface-tension effects are expected to be negligible for experiments involving an air–liquid interface, as in the work reported by Goller & Ranov (1968).

4.2. *Quasi-steady effects of acceleration and deceleration*

A series of experiments was performed to determine the behaviour of the water–oil interface under conditions of small steady acceleration or deceleration of the centrifuge. Electronic control circuits permit setting various acceleration or deceleration rates. A signal related to the bowl speed and an internally generated signal varying at a rate related to the desired acceleration or deceleration are compared and the difference is used to control the air supply to the air turbine.

During an experiment, pulses from the magnetic pick-up in the turbine head are counted over a 10 s interval. The resulting count is taken as the average rotational speed of the centrifuge for that time interval. The change in speed for successive 10 s intervals is a measure of the acceleration rate. The mean acceleration rate for a given experiment is obtained by averaging the rates, obtained as described above, over the

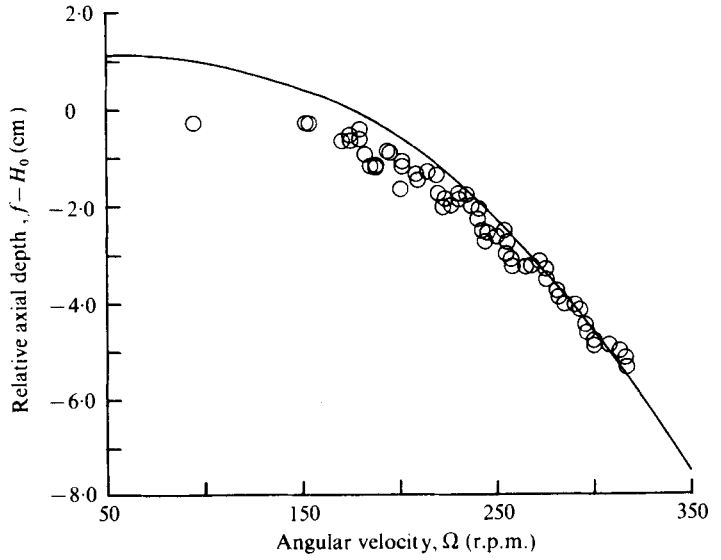

FIGURE 7. Interface axial depth for steady acceleration, water and 20 cS silicone oil, $H_0/H = 0{\cdot}6$, $\dot{\Omega}_{avg} = 0{\cdot}85$ r.p.m./s.

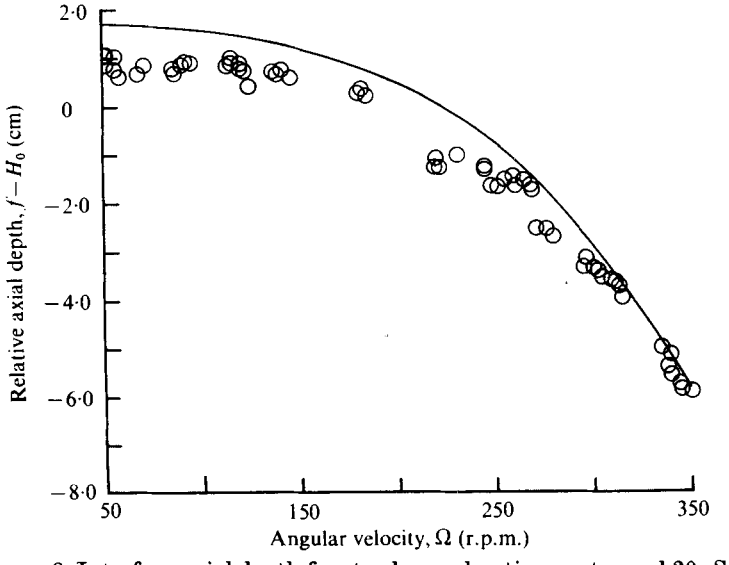

FIGURE 8. Interface axial depth for steady acceleration, water and 20 cS silicone oil, $H_0/H = 0{\cdot}6$, $\dot{\Omega}_{avg} = 0{\cdot}115$ r.p.m./s.

duration (about 30 min) of the experiment, thus averaging out any small fluctuations in the acceleration or deceleration rates induced by the speed control.

The experiments discussed below cover a range of rotational Froude numbers N_F from about 0·2 to 10, a range of internal Froude numbers N_I from about 4 to 400 and a range of characteristic time ratios β from about 0·1 to 0·5. The surface-tension parameter δ is less than 0·2 for both the 20 cS and the 350 cS oil. The surface shape para-

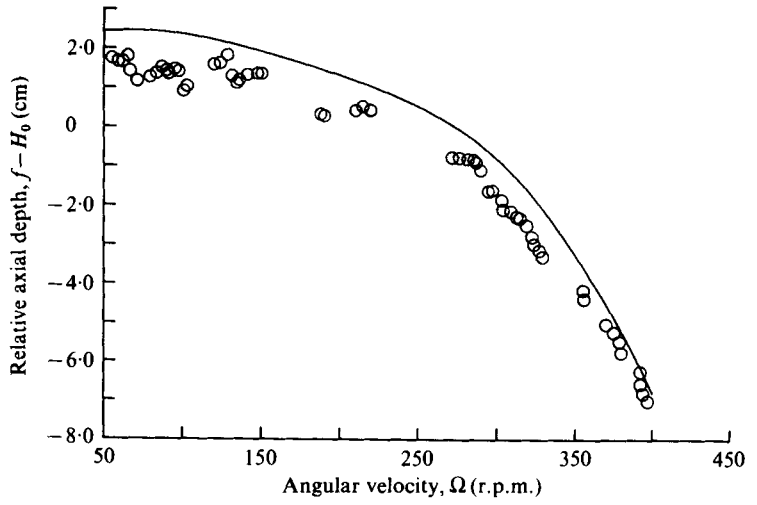

FIGURE 9. Interface axial depth for steady acceleration, water and 20 cS silicone oil, $H_0/H = 0{\cdot}6$, $\dot{\Omega}_{avg} = 0{\cdot}151$ r.p.m./s.

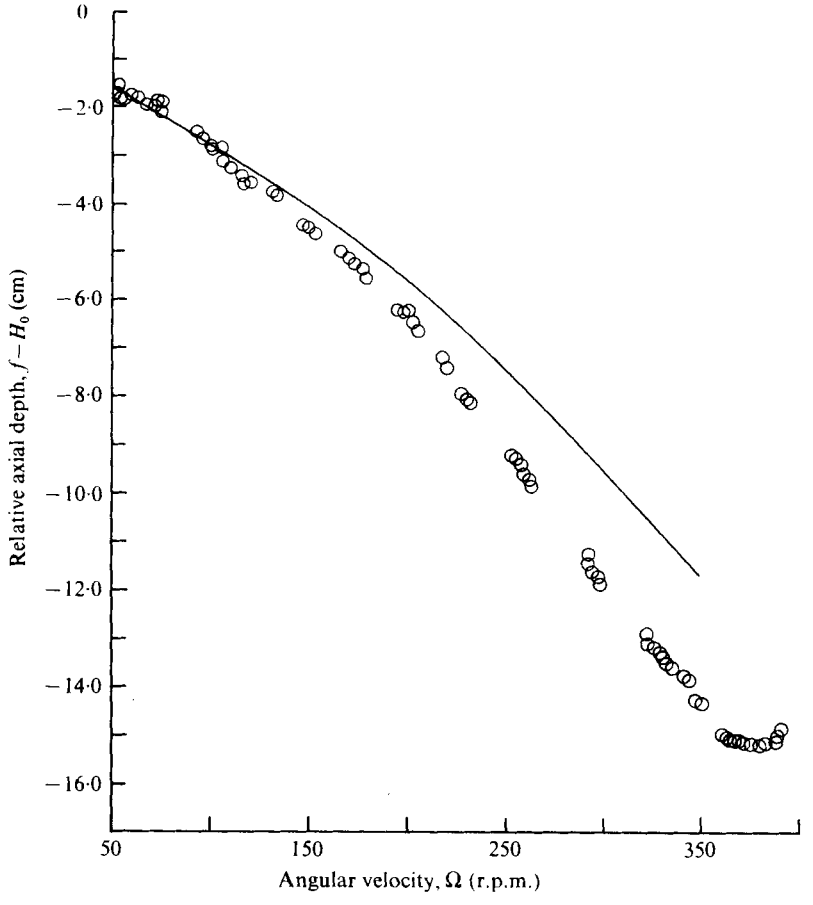

FIGURE 10. Interface axial depth for steady deceleration, water and 20 cS silicone oil, $H_0/H = 0{\cdot}6$, $\dot{\Omega}_{avg} = -0{\cdot}091$ r.p.m./s.

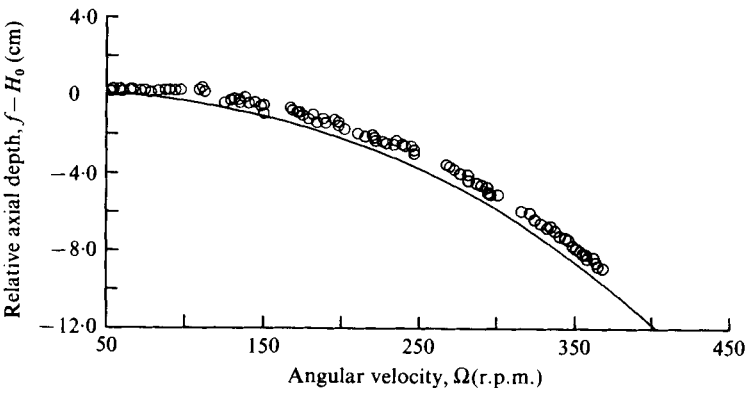

FIGURE 11. Interface axial depth for steady acceleration, water and 350 cS silicone oil, $H_0/H = 0{\cdot}25$, $\dot{\Omega}_{avg} = 0{\cdot}057$ r.p.m./s.

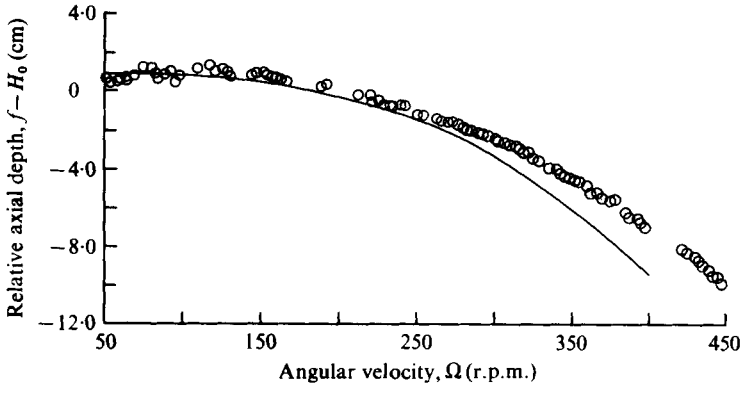

FIGURE 12. Interface axial depth for steady acceleration, water and 350 cS silicone oil, $H_0/H = 0{\cdot}25$, $\dot{\Omega}_{avg} = 0{\cdot}147$ r.p.m./s.

meter Γ ranges from about 0·2 to 2. Note that for some of our data β and Γ are larger than would seem reasonable for the perturbation scheme used in the analysis. Nevertheless, as indicated later, agreement between predictions and observations is good despite this fact.

The results of the experiments with water and 20 cS silicone oil at mean acceleration rates of 0·085, 0·115 and 0·151 r.p.m./s are shown in figures 7, 8 and 9. The result for a mean deceleration rate of $-0{\cdot}091$ r.p.m./s is presented in figure 10. These experiments were performed at an H_0/H of 0·6, where H_0 is the rest height of the interface and H is the total inside length of the bowl. The experimental results for water and 350 cS oil are shown in figures 11 and 12 for mean acceleration rates of 0·057 and 0·147 r.p.m./s, respectively, and $H_0/H = 0{\cdot}25$. In all figures, the depth of the axial interface point relative to its position when the bowl is at rest is shown as a function of rotational speed. Also shown in the figures are curves obtained from (55). These curves correspond to computations made with the mean acceleration or deceleration rate.

For all deceleration experiments, deceleration was started after the centrifuge had been rotating at a selected speed for a sufficiently long time to ensure rigid-body rotation of the contained fluids. After deceleration starts, some time must elapse

before the interface shape adjusts from that appropriate to rigid-body rotation to the shape associated with the imposed steady deceleration rate. This effect can be seen clearly in figure 10 by noting the deviation of the data points at high rotational speed from the trend of the remaining data. These points represent data obtained within the first few minutes after the start of deceleration. The time required for this transient phase to decay is estimated, from (29), to be 4·5–5 min, which is consistent with the time required for the transient adjustment of the interface, as estimated from the figures.

The results given in figure 7 are those from an acceleration experiment in which acceleration is started from a state of rigid-body rotation at low speed. The deviation of the data point at the lowest rotational speed is again associated with the time required to achieve an interface shape appropriate to the imposed acceleration rate.

In many of the figures under discussion, cyclic deviation between the data and the computed curves seems to be present. Such variation is associated with pressure variations in the primary air supply tank which result from the on–off cycle of the air compressor.

The agreement between experimentally measured depths and those predicted from the analysis is good even for data obtained under conditions which are outside those for which the perturbation analysis might be expected to be reasonable. The ranges of Ω and $\dot{\Omega}$ for which we expect the perturbation analysis to be valid can be determined from figures 4 and 5. These figures are contour plots, drawn in Ω, $\dot{\Omega}$ space, giving regions in which the sum of the correction terms $F^{(1)}$, ..., $F^{(4)}$ of the perturbation expansion is within a certain percentage of the zero-order solution $F^{(0)}$. Figure 4 applies to water and 20 cS oil at $H/H_0 = 0{\cdot}6$ and figure 5 applies to water and 350 cS oil at $H/H_0 = 0{\cdot}25$. The fact that relatively good experimental agreement is sometimes achieved in regions where the correction terms are relatively large seems to indicate that the corrections of higher order than those included in the perturbation analysis can be small under some conditions.

4.3. *Transient effects and stability*

A brief study of the transient effects discussed in the analysis section was carried out for both step spin-up (§2.2) and the decay of transients (§2.1).

For step spin-up, the centrifuge was automatically set at some given speed (corresponding to $\Omega - \Delta\Omega$ in the analysis) and the fluids allowed to attain rigid-body rotation at that speed. At $t = 0$, the speed of the centrifuge was suddenly increased by an amount $\Delta\Omega$ chosen to increase the bowl speed by 5 or 10 %. The centrifuge was then maintained at this new speed. The axial height of the interface was observed first to rise to some maximum height and then to decay to that of rigid-body rotation at the new speed. Figure 15 (plate 2) shows a photograph of the interface shape at its maximum axial height. The fluids are water and 350 cS oil at a speed of 204 r.p.m. for a $\Delta\Omega/\Omega$ of 0·1. Figure 2 shows the predicted shape of the interface at its maximum rise for the same case, calculated from (44). The calculated shape of the interface can be seen to possess the same qualitative features as are observed experimentally. The shape of the interface for rigid rotation at $\Omega = 204$ r.p.m. is also shown in figure 2.

To obtain a quantitative comparison between theory and experiment, the maximum axial rise of the interface was measured for a variety of speeds and sudden changes in

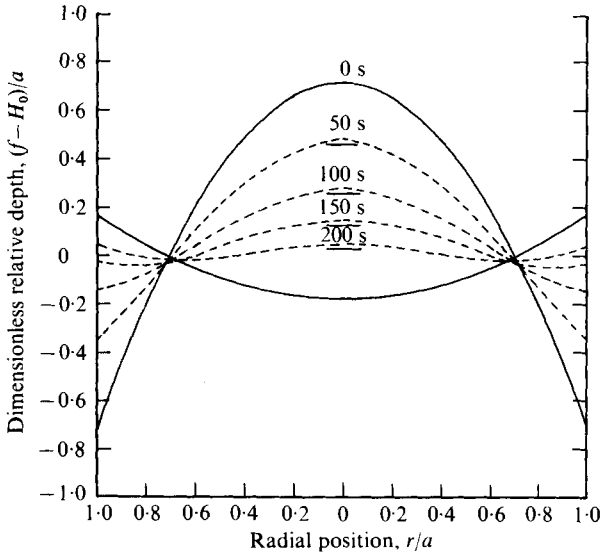

FIGURE 13. Decay of interface from a state of steady acceleration for water and 350 cS silicone oil. Computed from (29) at times $t = 0$, 50 s, 100 s, 150 s, 200 s and ∞. Solid curves denote shape of interface initially (at $t = 0$) and at $t = \infty$. Dashes on the axis indicate the observed interface axial depths at 50, 100, 150 and 200 s.

speed and compared with the rise calculated from (45). The results are shown in figure 3, where the dimensionless rise is plotted against $\lambda^{-\frac{1}{2}}$ [see (26)], which is proportional to Ω. The agreement is good below about 250 r.p.m. Above this speed the data lie somewhat below the predicted values. We believe that this is due to surface-tension effects on the interface shape, which at higher speeds has regions of large curvature. Such surface-tension effects have been neglected in the analysis leading up to the equation for the maximum axial rise.

To study the decay to rigid-body rotation, the centrifuge was accelerated from rest to about 100 r.p.m. at a rate selected so as to produce an interface shape which was convex downwards and of reasonable height. The acceleration was then stopped and the electronic controls set to maintain a constant speed of about 100 r.p.m. The height of the axial interface point was then measured at several times during the decay of the interface shape to the shape associated with rigid-body rotation at the selected constant speed. In addition, photographs were taken to observe the complete interface shape during the decay to rigid-body rotation. A series of photographs illustrating such a decay for water and 20 cS silicone oil is shown in figures 14(*a*)–(*e*) (plate 1). Figure 1 gives the corresponding behaviour of the interface computed from (29). A more quantitative comparison between the time dependence of the observed and calculated depth of the axial interface point is given in figure 13 for water and 350 cS oil. The higher viscosity oil was used in this experiment to approximate more closely the assumption of infinite viscosity of the upper fluid made in the analysis of the transient decay.

The agreement between the observed and predicted behaviour of the interface during the transient decay is surprisingly good in view of the fact that the analysis neglected surface tension and assumed infinite viscosity of the upper fluid.

During acceleration and deceleration studies it was observed that instabilities occurred at certain combinations of rotational speed and acceleration rate. During acceleration these instabilities manifest themselves initially as a wavelike deformation of the interface, clearly seen in figure 16 (plate 2). Continued acceleration after the appearance of such deformation results in a complete breakup of the interface.

In general, much higher deceleration rates were required to induce instability than was the case for acceleration. Higher acceleration rates from rest resulted in the appearance of instability at a lower rotational speed.

The authors gratefully acknowledge both the loan of the centrifuge and its auxilliary equipment and financial assistance, provided by Union Carbide Corporation, Nuclear Division, Oak Ridge, Tennessee.

REFERENCES

ANDERSON, N. G. 1966 The development of zonal centrifuges and ancillary systems for tissue fractionation and analysis. *Nat. Cancer Inst. Monograph* no. 21. U.S. Department Health, Education and Welfare, Public Health Service, Bethesda, Maryland.

GOLLER, H. & RANOV, T. 1968 Unsteady rotating flow in a cylinder with a free surface. *J. Basic Engng* **90**, 445.

GREENSPAN, H. P. 1969 *The Theory of Rotating Fluids.* Cambridge University Press.

HOLTON, J. R. 1965 The influence of viscous boundary layers on transient motions in a stratified rotating fluid. Part 1. *J. Atmos. Sci.* **22**, 402.

PEDLOSKY, J. 1967 The spin up of a stratified fluid. *J. Fluid Mech.* **28**, 463.

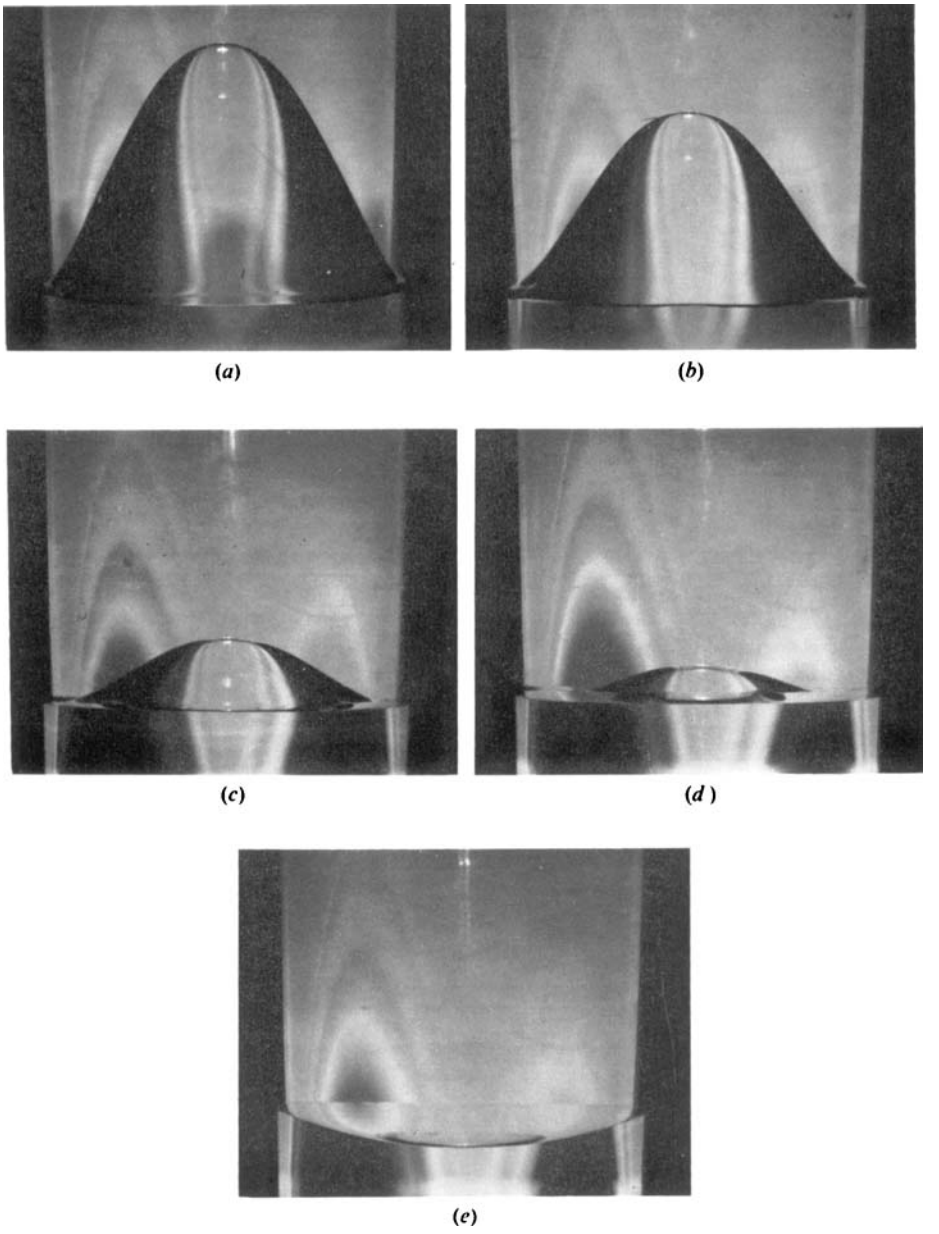

FIGURE 14. Decay of interface shape from a state of steady acceleration to rigid-body rotation at $\Omega = 100$ r.p.m. (*a*) Interface at cessation of acceleration; $t = 0$. (*b*) Interface at 50 s. (*c*) Interface at 100 s. (*d*) Interface at 150 s. (*e*) Interface in rigid-body rotation.

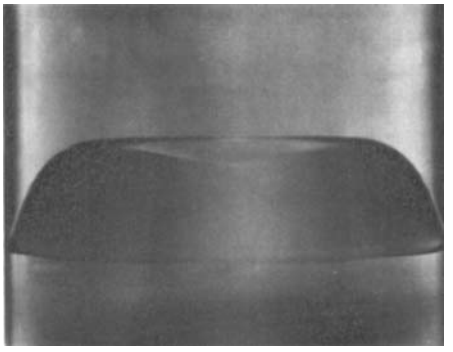

FIGURE 15. Short-time asymptotic interface shape for step spin-up of water and 350 cS silicone oil; $\Omega = 204$ r.p.m., $\dot{\Omega} = 0{\cdot}1$ r.p.m./s, $H_0/H = 0{\cdot}5$.

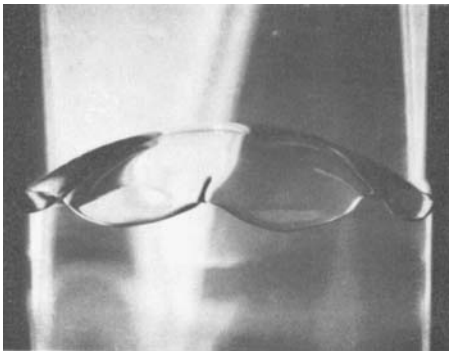

FIGURE 16. Onset of interfacial instability during steady acceleration of water and 20 cS silicone oil; $\Omega = 40$ r.p.m., $\dot{\Omega} = 2{\cdot}0$ r.p.m./s.